Anomalous scattering analysis of *Agrobacterium radiobacter* phosphotriesterase: the prominent role of iron in the heterobinuclear active site

Colin J. JACKSON[*][1], Paul D. CARR[*][1], Hye-Kyung KIM[*], Jian-Wei LIU[*], Paul HERRALD†, Nataša MITIĆ†, Gerhard SCHENK†, Clyde A. SMITH‡ and David L. OLLIS[*][2]

*Research School of Chemistry, Building 35, Australian National University, Canberra, ACT 0200, Australia, †School of Molecular and Microbial Sciences, University of Queensland, St. Lucia Campus, Brisbane, QLD 4072, Australia, and ‡Stanford Linear Accelerator Center/Stanford Synchrotron Radiation Laboratory (SLAC/SSRL), MS:99, 2575 Sand Hill Road, Menlo Park, CA 94025, U.S.A.

Bacterial phosphotriesterases are binuclear metalloproteins for which the catalytic mechanism has been studied with a variety of techniques, principally using active sites reconstituted *in vitro* from apoenzymes. Here, atomic absorption spectroscopy and anomalous X-ray scattering have been used to determine the identity of the metals incorporated into the active site *in vivo*. We have recombinantly expressed the phosphotriesterase from *Agrobacterium radiobacter* (OpdA) in *Escherichia coli* grown in medium supplemented with 1 mM CoCl$_2$ and in unsupplemented medium. Anomalous scattering data, collected from a single crystal at the Fe–K, Co–K and Zn–K edges, indicate that iron and cobalt are the primary constituents of the two metal-binding sites in the catalytic centre (α and β) in the protein expressed in *E. coli* grown in supplemented medium. Comparison with OpdA expressed in unsupplemented medium demonstrates that the cobalt present in the supplemented medium replaced zinc at the β-position of the active site, which results in an increase in the catalytic efficiency of the enzyme. These results suggest an essential role for iron in the catalytic mechanism of bacterial phosphotriesterases, and that these phosphotriesterases are natively heterobinuclear iron–zinc enzymes.

Key words: *Agrobacterium radiobacter*, anomalous scattering, heterobinuclear, iron–zinc, metallophosphoesterase, phosphotriesterase.

INTRODUCTION

The bacterial phosphotriesterases are members of a relatively small group of binuclear metallohydrolases that catalyse the hydrolysis of organophosphate triesters (EC 3.1.8.1). The toxicity of organophosphate triesters, and their use in agriculture as pesticides, means occupational or intentional exposure is a significant health hazard [1]. An enzyme (OpdA) capable of rapidly hydrolysing a phosphotriester bond in these compounds, thereby detoxifying them, has been isolated from an *Agrobacterium radiobacter* strain [2]. Because of the potential use of this enzyme in the detoxification of organophosphate pesticides, there is considerable interest in better understanding its catalytic mechanism and improving its efficiency.

The structure of OpdA, determined for crystals grown in Co^{2+}-supplemented medium, has been solved in the presence and absence of various products and inhibitors [3,4]. OpdA adopts an $(\alpha/\beta)_8$ barrel structure with a binuclear metal centre at the active site. A carboxylated lysine residue and a hydroxide ion bridge the metal ions. The co-ordination environment of the two metal ions varies according to the crystallization conditions. The invariant metal-ion ligands are shown in Figure 1, demonstrating that the α-site is more symmetrical, owing to the presence of Asp^{301}. Further co-ordination has been found to depend on the crystallization conditions. In the absence of products or inhibitors, both metal ions are co-ordinated in a distorted octahedral arrangement, with the addition of terminal ligands at each metal (a water/hydroxide at the β-site and ethylene glycol at the α-site), and a second water molecule 2.5 Å (1 Å = 0.1 nm) from the β-metal ion in an axial position. In the structure of an OpdA–DMTP (OpdA–dimethyl thiophosphate) complex, the β-metal is co-ordinated in a trigonal bipyramidal arrangement, with the equatorial (terminal) water/hydroxide ligand replaced by the sulphur atom of DMTP, and the movement of Arg^{254} in the second co-ordination sphere displacing the axial water ligand [4]. PTE, the homologous enzyme from *Pseudomonas diminuta*, in which all metal-ion-co-ordinating residues are conserved, has also been extensively studied using crystallography [5]. The co-ordination geometry of the α-metal in PTE crystallized with Zn^{2+} in the active site is best described as a distorted trigonal bipyramid, owing to the lack of the terminally co-ordinated ligand observed in the OpdA structures at this position. We have previously suggested that differences in the first co-ordination spheres of OpdA and PTE may be a consequence of the presence of different metals in the active site [4].

Both OpdA and PTE are catalytically active with a variety of metal ions (Zn^{2+}, Mn^{2+}, Co^{2+} or Cd^{2+}) [3,6]. Most of the physical characterization of PTE has been accomplished with Zn^{2+} in the active site, although both enzymes are more active toward phosphothionate compounds with Co^{2+} in the active site [3,6]. The mechanism of substrate hydrolysis is proposed to involve monodentate co-ordination of the substrate to the β-metal ion, followed by nucleophilic attack from a water/hydroxide molecule terminally co-ordinated to the α-metal ion [7]. This is consistent
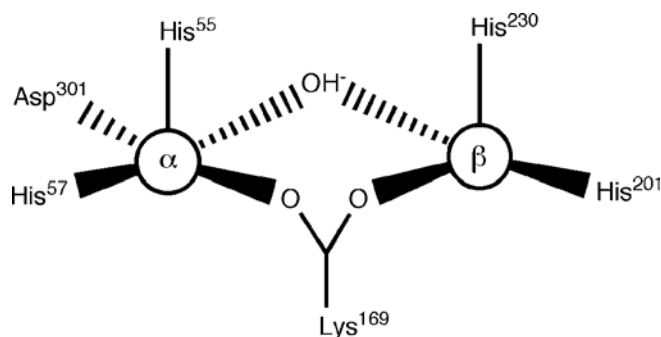

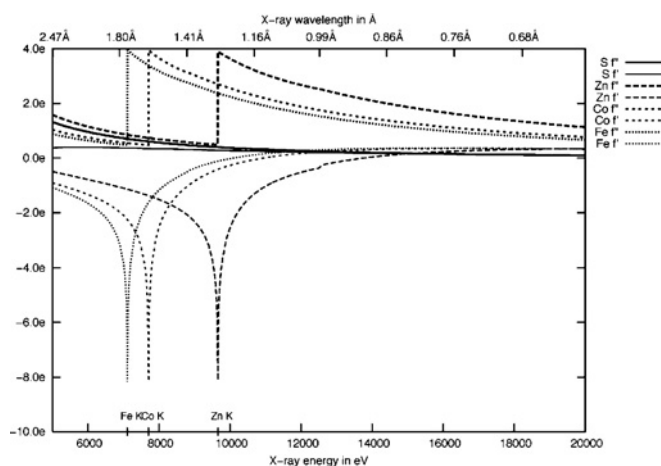**Figure 1   Schematic representation of the active site of OpdA**

Figure 2   Plot of the values of theoretical anomalous dispersion and absorption coefficients (f' and f'') for Fe, Co, Zn and S (sulphur) versus wavelength (Å) and energy (eV)

with: (i) kinetic studies that have demonstrated that the α-metal determines the strength of the attacking nucleophile, while the β-metal affects substrate binding [8], and (ii) crystallographic studies that have unequivocally demonstrated the production of the product, dimethyl thiophosphate, dually bound to the two metals without disruption to the bridging hydroxide [4]. Further work has demonstrated that catalysis can occur rapidly, in a one-step S_N2 reaction, or via intermediates in an addition–elimination reaction [7].

Field trials of OpdA as a bioremediation agent have been conducted [9], and it is already in use as a commercial product to detoxify organophosphates, sold under the brand name LandGuard™ from Orica Watercare (Melbourne, Vic, Australia). Removal of the metals from the active site using chelating agents such as EDTA, and reconstitution with known metal ions, is the most accurate method of controlling the identity of the metal ions at the active site. However, commercial production of proteins typically involves large-scale industrial fermentation and the removal of unlysed cells. Accordingly, it is important to understand which metal ions are incorporated into the active site when it is recombinantly expressed, as this can direct efforts toward improving the efficiency of the enzyme.

The collection of diffraction data at wavelengths corresponding to the absorption edges of particular metals is a valuable technique for their identification [10]. Transition metals, such as iron, cobalt and zinc, have absorption edges in the accessible range for collection of diffraction data at synchrotron beamlines (Figure 2) [11]. The metal ions present in the active site of the bacterial

phosphotriesterases have an important impact upon their activity [12]. It is therefore important, for the development of OpdA as a bioremediation agent, to distinguish which metals are present in the recombinantly expressed protein, and whether they have a preference for the α or β site. Consequently, we have collected anomalous dispersion data from a single OpdA crystal at the Fe–K, Co–K and Zn–K absorption edges. The goal of the present study was to ascertain the identity of the metal ions at each site and to relate this information to our current knowledge of structure–function relationships in OpdA.

EXPERIMENTAL

Materials

All chemicals were purchased from Sigma–Aldrich unless otherwise noted. Methyl parathion (O,O-dimethyl O-p-nitrophenyl phosphorothioate) was purchased from Chem Service Inc. (West Chester, PA, U.S.A.). The purity of the organophosphate was > 95 % according to the manufacturers. Bacto-tryptone and Bacto-yeast extract were purchased from Difco Laboratories. Molecular-biology reagents were purchased from New England Biolabs (via Genesearch Pty. Ltd, Arundel, QLD 4214, Australia) or Roche Diagnostics Australia Pty. Ltd. (Castle Hill, NSW, Australia) unless otherwise stated. Chromatography resins were purchased from Amersham Pharmacia Biotech AB (Uppsala, Sweden).

Bacterial strains and plasmids

Construction of the plasmid (pCy76-opdA) used to express OpdA [NCBI (National Center for Biotechnology Information) protein sequence database accession number: AAK85308] has been described previously [3]. The protein was expressed in *Escherichia coli* DH5α cells (Invitrogen).

Protein expression, purification and crystallization

Electrocompetent *E. coli* DH5α cells were transformed with the plasmid pCy76-opdA by electroporation, and a 20 ml starter culture in LB (Luria–Bertani) medium (supplemented with 50 μg/ml ampicillin) was inoculated, then incubated at 30 °C for 8 h. For the purpose of direct comparison, 100 μl of the same starter culture was used to inoculate two large-scale cultures in parallel, namely unsupplemented LB medium (10 g/l tryptone, 5 g/l yeast extract, 10 g/l NaCl, pH 7.0, and 50 μg/ml ampicillin), and TB (Terrific broth) medium (24 g/l of yeast extract, 12 g/l of tryptone, 100 mM K_2HPO_4/KH_2PO_4, pH 7.0, 0.4 % glycerol, and 50 μg/ml ampicillin) supplemented with 1 mM $CoCl_2$. Both cultures were incubated at 37 °C for 30 h. Expression of OpdA from pCy76 is constitutive. Excess $CoCl_2$ in LB medium was inhibitory to cell growth, hence the need to use TB growth medium for expression in the presence of 1 mM $CoCl_2$.

Cells were harvested and resuspended in 50 mM Hepes buffer, pH 8.0. Cell lysis was achieved using a French Press, and cell debris was separated from the soluble fraction by centrifugation at 30 000 $\boldsymbol{g}$ for 30 min, followed by filtration through a 0.45 μm-pore-size nitrocellulose membrane (Millipore). The soluble fraction was loaded on to a DEAE Fractogel column. OpdA did not bind to the column, and was collected in the flow-through material. The protein was then dialysed against 50 mM Hepes, pH 7.0, for 12 h, and loaded on to an SP (sulphopropyl)-Sepharose column. Bound OpdA was eluted at approx. 150 mM NaCl using a linear gradient from 0 to 1 M. SDS/PAGE analysis of the eluted OpdA indicated a purity of greater than 95 %. The protein was stored at 4 °C in 50 mM Hepes (pH 7.0)/150 mM NaCl.
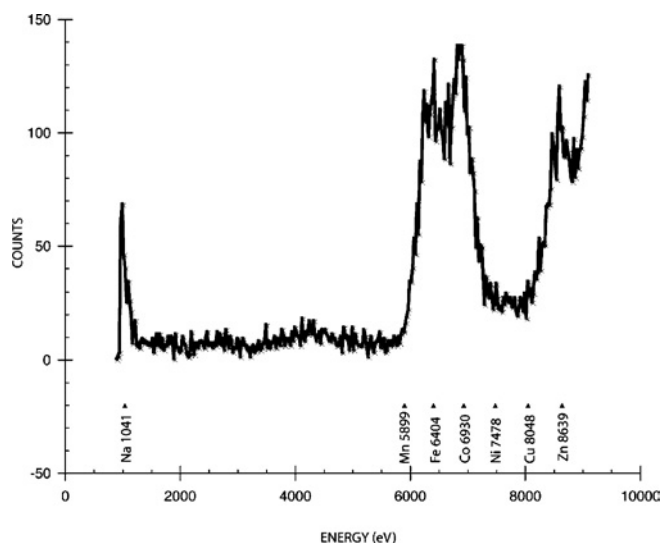
Figure 3   Excitation fluorescence scan performed on a single crystal of OpdA

OpdA was dialysed against 50 mM Hepes pH 7.0, 150 mM NaCl, 1 mM $CoCl_2$ and concentrated via ultrafiltration to 6.4 mg/ml for crystallization. Protein concentrations were measured by UV absorption at 280 nm. The absorption coefficient for OpdA was calculated as 29 280 $M^{-1} \cdot cm^{-1}$ [3].

Crystals were grown in hanging drops using vapour diffusion. Drops were made by mixing 5 μl of protein solution with 5 μl of a reservoir solution that consisted of 20 % (w/v) PEG-3350 [poly-(ethylene glycol)-3350]/0.2 M sodium nitrate. We were unable to obtain crystals of OpdA purified from unsupplemented media.

X-ray data collection

OpdA crystals were transferred to a cryobuffer solution that consisted of the crystallization buffer with 40 % PEG-3350, and flash-cooled to 100 K on an Oxford Cryostream (Oxford Cryosystems, Long Hanborough, Oxford, U.K.) apparatus. The crystals were then transferred to a Taylor Wharton CX100 dry shipper at 77 K for transport to beamline 9-2 on the synchrotron at the Stanford Synchrotron Radiation Laboratory [(SSRL) Menlo Park, CA, U.S.A.]. Data were collected remotely from Australia using Blue-Ice and NX-Client/Server software. An excitation fluorescence

spectrum of the crystal was recorded to check for the presence of various metal ions (Figure 3). Individual fluorescence scans were then performed to ascertain the precise energies of the absorption edges. Complete X-ray anomalous datasets, consisting of $180 \times 1°$ oscillations, were collected at the Fe–K (7131.80 eV), Co–K (7724.88 eV) and Zn–K (9576.29 eV) edges from a single OpdA crystal to 1.9 Å resolution (Table 1). Data integration, scaling and reduction were performed using the programs MOSFLM and SCALA [13,14]. This was again performed on SSRL computers remotely from Australia. Data collection statistics are given in Table 1.

Refinement

The crystal cell parameters (Table 1) were found to be iso-morphous with a previously solved structure (2D2J) [4]. The asymmetric unit contained a single monomer of the enzyme. Initial protein phases were calculated using the refined OpdA structure as a model. Refinement was undertaken using the program REFMAC [15], as implemented in the CCP4 suite of programs [16]. The structure of ethylene glycol was taken from the previous study [4].

Anomalous scattering analysis

The fast-Fourier-transform application from the CCP4 suite of programs was used to construct BDFMs (Bijvoet difference Fourier maps) [17], using the anomalous data collected at each wavelength. These maps were calculated using the phases from the structure refined against the data collected at 7131.8 eV. The intensities of the anomalous peaks at each metal site ($e/Å^3$) were determined using the program Coot [18]. As an internal standard, the intensity of an anomalous peak corresponding to the sulphur atom from Met[325] was also determined. This was then used to scale the intensity of the peaks to account for the variation in incident X-ray intensity at the three different wavelengths, taking into account the theoretical reduction of the anomalous sulphur signal with wavelength. Theoretical anomalous dispersion and absorption coefficients (f' and f'') for Fe, Co, Zn and S were derived using the theoretical approximation developed by Cromer and Liberman [19] (Table 2), and the scattering data used to generate the plot of f' and f'' versus wavelength (Figure 2) were calculated using the subroutine library by Brennan and Cowan [19a], as implemented at the Biomolecular Structure Center web interface (http://skuld.bmsc.washington.edu/scatter/).

Table 1   Data collection statistics for OpdA at 7132, 7725 and 9576 eV

Parameter	Edge …	Value		
		Fe–K (7132 eV)	Co–K (7725 eV)	Zn–K (9576 eV)
Space group		$P3_121$ $a = 108.9, c = 62.4$ Å	$P3_121$ $a = 108.9, c = 62.4$ Å	$P3_121$ $a = 108.9, c = 62.4$ Å
Number of observations		351 555	360 482	368 460
Number of unique reflections		33 940	33 957	33 964
Completeness (%)		100	100	100
$\langle I/\sigma(I)\rangle$		29.9	30.7	31.0
Resolution range (Å)				
Overall		62.0–1.9	62.0–1.9	62.0–1.9
Outer		2.0–1.9	2.0–1.9	2.0–1.9
R_{scal} (overall/outer shell)		6.3/23.0	6.2/22.9	6.1/20.7

Table 2   (a) Electron density ($e/\text{Å}^3$) at the α and β metal sites, measured from the BDFMs and (b) AAS metal-ion analysis of OpdA expressed in supplemented ($+\text{CoCl}_2$) and unsupplemented ($-\text{CoCl}_2$) media

(**a**) The corrected values were scaled using the anomalous scattering for the Met[325] sulphur atom as an internal standard to account for different incident intensities at the various wavelengths. Electron density is shown, after removal of residual anomalous scattering for the other absorption edges, with the ratio of electron density per metal in parenthesis. (**b**) Ratios of metals are shown in parenthesis.

(a) Anomalous scattering

	Value		
Metal edge ...	Fe–K (7132 eV)	Co–K (7725 eV)	Zn–K (9576 eV)
α			
$e/\text{Å}^3$	0.77	0.61	0.50
Corrected	0.77	0.64	0.63
β			
$e/\text{Å}^3$	0.21	0.69	0.39
Corrected	0.21	0.72	0.50
Theoretical anomalous signal (%)*			
Fe	100	86	61
Co	14	100	69
Zn	22	19	100
Electron density (without residual anomalous signal)			
α	0.77	0.00	0.16
β	0.13	0.62	0.20
Total ...	0.90 (1)	0.62 (0.69)	0.36 (0.40)

(b) AAS

Ratio (total/mol)			
$+\text{CoCl}_2$	0.93 ± 0.03 (1)	0.65 ± 0.03 (0.70)	0.32 ± 0.01 (0.34)
$-\text{CoCl}_2$	0.53 ± 0.02 (1)	0.00 ± 0.00 (0.00)	0.47 ± 0.02 (0.89)

* Theoretical f' values are also shown to indicate the level of residual scattering; edge values were calculated at the edge, and off-edge values at the nearest 100 eV.

Metal analysis by AAS (atomic absorption spectroscopy)

The content of protein-bound metal ions was determined in triplicate by AAS using a Varian SpectrAA 220FS instrument. Standard solutions for iron, cobalt and zinc, ranging in concentration from 20 to 100 p.p.b. (parts per billion), were prepared from analytical stock solutions (Merck) using MilliQ water. Protein samples were diluted with desalted buffer (50 mM Hepes, pH 7.0). This buffer and MilliQ water were used as controls in AAS measurements; no measurable quantities of metal ions were detected. The estimated error for each metal ion was less than 5 % (Table 2).

Measurement of enzyme activity and kinetic parameters

Activity measurements on crude extracts were carried out in triplicates to determine the level of phosphotriesterase activity in supplemented and unsupplemented cultures expressing OpdA. A 1–10 μl portion of cell culture was added to a 1 ml reaction mix containing 250 μM methyl parathion, 100 mM Ches [2-(*N*-cyclohexylamino)ethanesulphonic acid], pH 9.1, 10 % (v/v) methanol, 2.5 % (w/v) PEG-8000, and 1 % of the cell lysis reagent BugBuster (Novagen). The specific activity was determined by measuring the release of 4-nitrophenolate ($\varepsilon = 16\,600\ \text{M}^{-1} \cdot \text{cm}^{-1}$) spectrophotometrically, using a Varian Cary 1E UV–visible spectrophotometer.

Kinetic parameters for purified OpdA were determined by varying the concentration of methyl parathion from 31.25 to 1000 μM. Because of the poor solubility of methyl parathion,
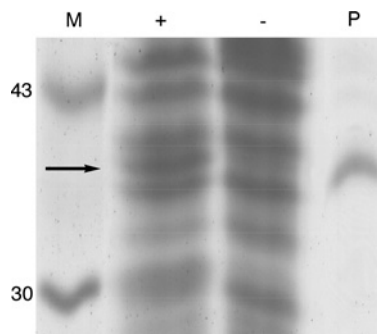
Figure 4   SDS/PAGE analysis of the expression of OpdA in TB media supplemented by 1 mM CoCl_2 (+) or in unsupplemented LB media (−)

Purified OpdA (P) and molecular-mass markers (M) are also shown. Values on the extreme left are molecular masses in kDa.

this was the largest substrate concentration range achievable. The reaction mixture contained 10 % methanol, 2.5 % PEG-8000, 100 mM Ches, pH 9.1, and 1 mg/ml BSA. All measurements were made in duplicate. The values for V_max and K_m were determined from a fit of the data to eqn (1):

$$v = V_\text{max}A/(K_\text{m} + A) \qquad (1)$$

where v is the initial velocity, V_max is the maximum velocity, K_m is the Michaelis constant and A is the substrate concentration. The k_cat was calculated by dividing V_max by the concentration of enzyme ([E]) used in the reaction according to the equation:

$$V_\text{max} = k_\text{cat}[\text{E}]$$

Metal-ion addition

To determine whether ferrous or ferric iron is required for activity, metal-ion-addition studies were performed. OpdA expressed and purified from unsupplemented medium was transferred to a solution containing 1 mM ascorbic acid/100 mM Hepes, pH 7.9, with either 10 mM FeSO_4, 10 mM $\text{Fe(NO}_3)_3$, or no exogenous metal. Following an incubation period of 1 h at room temperature (25 °C), an aliquot was then diluted 30-fold in the assay mix, which contained 250 μM methyl parathion, 100 mM Ches, pH 9.1, 10 % methanol and 2.5 % PEG-8000. Absorbance changes at 405 nm were measured with a plate reader (Thermo Labsystems, Franklin, MA, U.S.A.) at 10 s intervals.

RESULTS

Protein expression and purification

We sought to determine whether the growth medium would affect the level of OpdA expression. SDS/PAGE analysis demonstrates that OpdA is expressed at higher levels in TB medium supplemented with 1 mM CoCl_2 than in unsupplemented LB medium (Figure 4). This is consistent with the yield of purified protein from each culture: supplemented TB produced 4.9 mg of soluble OpdA/litre, and unsupplemented LB produced 1.8 mg/litre (Table 3).

Determination of specific activity and kinetic parameters

The calculated phosphotriesterase activities of the TB and LB cultures are shown in Table 3. The level of activity in the supplemented culture was approx. 14-fold higher than that in the unsupplemented culture. Because a cell-lysis agent, BugBuster,

Table 3   Yield of soluble protein, specific activity and kinetic parameters for the hydrolysis of methyl parathion by OpdA expressed in the presence (+) or absence (−) of $CoCl_2$

Protein	Activity (μM/min per μl of culture)	Soluble protein (mg/l)	Specific activity (units/mg)	k_{cat} (s^{-1})	K_m (M)	k_{cat}/K_m ($s^{-1} \cdot M^{-1}$)
OpdA + Co^{2+}	1.94 ± 0.12	4.9	168 ± 3	1180 ± 80	$3.6 \times 10^{-4} \pm 0.6 \times 10^{-4}$	$3.3 \times 10^{6} \pm 0.8 \times 10^{6}$
OpdA − Co^{2+}	0.14 ± 0.01	1.8	34 ± 1	255 ± 16	$4.1 \times 10^{-4} \pm 0.6 \times 10^{-4}$	$6.3 \times 10^{5} \pm 1.3 \times 10^{5}$

Table 4   Refinement statistics for data collected at 7132 eV

Parameter	Value
Resolution range (Å)	
Overall	62.0–1.9
Outer shell	2.0–1.9
Reflections	
Working set	32 249
Test set	1668
R/R_{free} (%)	17.4/20.4
Number of:	
Protein atoms	2511
Water molecules	241
Metal ions	2
Ethylene glycol molecules	2
Root mean square deviation from target bonds	
Lengths (Å)	0.015
Bonds (°)	1.394
B-factors (Å^2)	
Main chain	19.6
Side chain	22.0
Metals	24.4
Waters	32.1
Ramachandran plot (%)	
Most favoured region	89.7
Additionally allowed	9.9
Generously allowed	0.4
Disallowed	0

was included in the reaction mixture, these measurements were not affected by transport or diffusion of parathion across the cell membrane.

The specific activities, and values of k_{cat}, K_m and k_{cat}/K_m, for purified OpdA, determined by fitting the data to eqn (1), are also shown in Table 3. These results demonstrate that the catalytic efficiency of the enzyme is enhanced when it is expressed in enriched medium supplemented with 1 mM $CoCl_2$, as indicted by an approx. 5-fold increase in the k_{cat} and k_{cat}/K_m; the K_m value is not significantly affected by changes in the growth medium.

Metal analysis by AAS

The content of iron, zinc and cobalt in OpdA purified from the $CoCl_2$-supplemented medium was 0.93, 0.32 and 0.65 atom per active site (1: 0.35: 0.7) respectively (Table 2). In contrast, OpdA purified from the unsupplemented medium contained 0.53 Fe and 0.47 Zn atom per active site (1:0.9), with the amount of cobalt below the limit of detection. Thus OpdA from unsupplemented medium had half the metal content of the fully occupied active site of OpdA purified from supplemented medium. Additionally, it is evident that the addition of Co^{2+} to the growth medium results in the replacement of Zn^{2+}, with the relative amount of Zn^{2+} decreasing from 0.9 to 0.35 and that of Co increasing from 0 to 0.7, relative to iron.

Quality of the crystal structure

The overall structure is essentially identical with that previously solved (2D2J) [4]. These data were refined principally to provide phases for the construction of anomalous difference maps and there is no new structural information to report. Data collection and refinement statistics are listed in Table 4 and indicate that the data and refinement are robust.

Anomalous X-ray scattering

The excitation fluorescence scan, shown in Figure 3, demonstrates that the only metals present in significant concentrations in the crystal are sodium, iron, cobalt and zinc. The presence of sodium is an artefact due to the crystallization conditions and cryoprotectant. Data were collected at the Fe–K, Co–K and Zn–K edges. Figures 5 and 6 show anomalous difference Patterson maps and BDFMs calculated from the data collected at these wavelengths. The electron densities of the anomalous peaks are listed in Table 2(a) alongside corrected values to account for differences in the incident radiation intensity. The theoretical anomalous
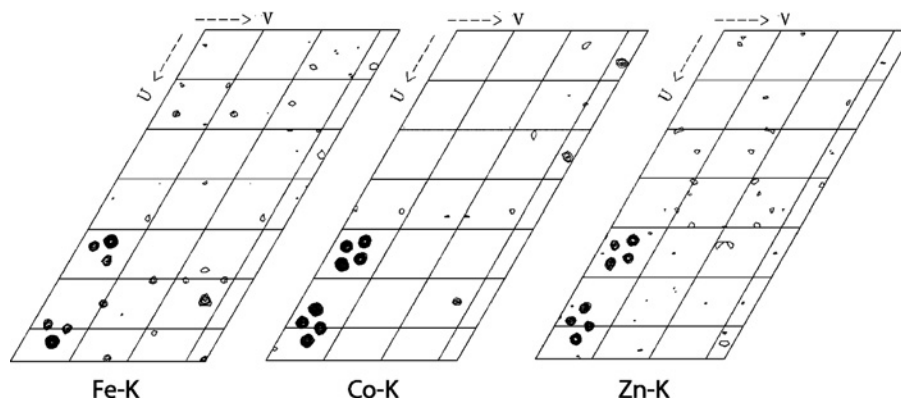
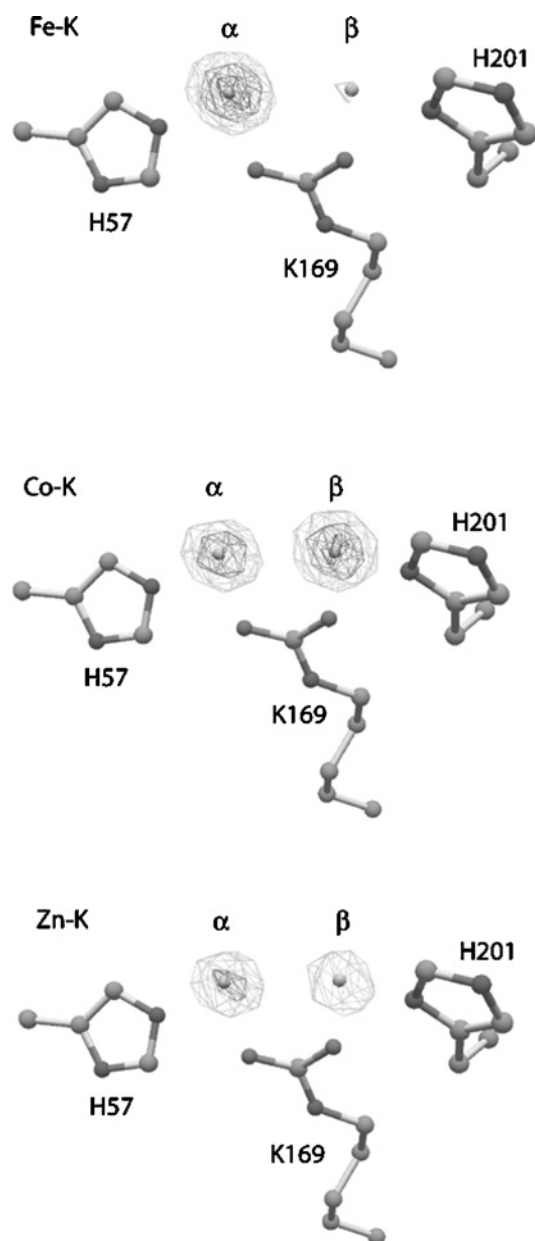**Figure 5   Anomalous difference Patterson map displaying the $Z = 2/3$ Harker section**

Figure 6   BDFMs contoured at 20 and 40 σ for data collected at the Fe–K, Co–K and Zn–K edges

dispersion coefficients at wavelengths close to the energies used (Figure 2) are also shown. These were used to subtract the residual anomalous signal from all edges to provide an estimate of the relative metal concentrations. It is clear that the residual absorption from Fe at the α-site accounts for the most of the density at 7725 eV and a significant proportion of the density at 9576 eV. This indicates that at least 80 % of the metal ion at this position is iron, with a small amount of zinc present. The densities at the β-site also appear to be dominated by a single metal ion: residual absorption from the high proportion of cobalt accounts for the density at 9576 eV, and a significant amount of the density at 7132 eV. This indicates that the primary constituent of the β-site is cobalt, with a small amount of iron ($\sim 15\%$) and zinc ($\sim 20\%$) present. This is in very good agreement with the AAS measurements summarized in Table 2(b). The anomalous scattering is shown graphically in Figure 6: electron density at
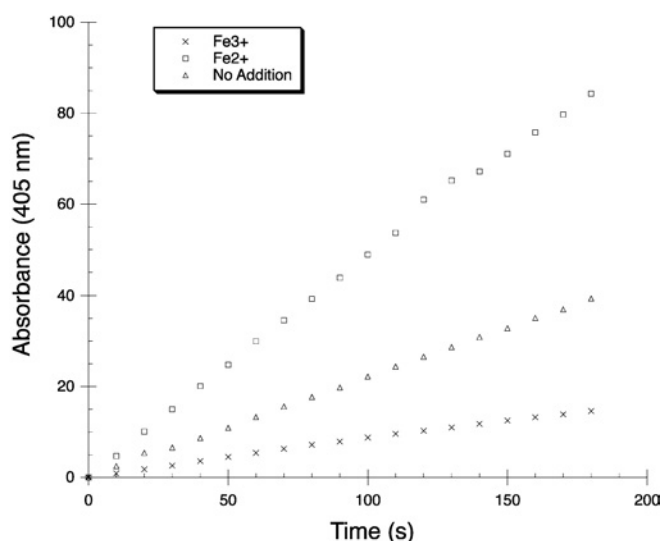
Figure 7   Relative activity of OpdA with or without addition of Fe^{2+} or Fe^{3+}

the Fe–K edge (7131.8 eV) is about four times higher at the α-site relative to the β-site. The density at the β-site then increases $\sim$3-fold upon moving to the Co–K edge (7724.9 eV). Irrespective of the stoichiometry of the minor metals at each position, the data provide an unequivocal indication that iron and cobalt occupy the majority of the α and β positions respectively.

Metal-ion addition

In order to examine whether OpdA is active with Fe^{2+} or Fe^{3+} ions in the active site, OpdA that had been expressed in, and purified from, unsupplemented medium was transferred to a solution containing either 10 mM $FeSO_4$ (Fe^{2+}) or 10 mM $Fe(NO_3)_3$ (Fe^{3+}) before the activity was measured by monitoring changes in specific activity over several minutes (Figure 7). The addition of Fe^{2+} increases the activity approx. 2-fold in comparison with the control (no added metal ions), whereas adding Fe^{3+} inhibits the activity $\sim$4-fold. This observation demonstrates that OpdA requires iron to be in the bivalent (ferrous) state for catalytic activity.

DISCUSSION

The level of OpdA expression, and the specific activity of the enzyme, is enhanced through the use of TB medium supplemented with 1 mM $CoCl_2$ (Figure 4 and Table 3). The addition of metal ions has previously been shown to enhance the specific activity of PTE expressed in *E. coli* [20]. A more recent study demonstrated that the expression of PTE in *E. coli* was not affected by the addition of cobalt, and concluded that the enhancement of activity in cultures grown in supplemented medium is a result of the conversion of apo-PTE into dimetal-PTE [21]. Our results agree with some aspects of this. OpdA purified from unsupplemented medium had a metal content ratio of 1 per enzyme molecule; because metals add pairwise to the bacterial phosphotriesterases [22], this indicates that half the purified enzyme consisted of inactive apo-OpdA. By contrast, the metal-ion content of OpdA purified from supplemented medium is 1.9 per enzyme molecule (Table 2b), indicating that most of the purified enzyme molecules are in the active (dimetal) form. However, we have also found that the expression level and yield of soluble protein are higher in supplemented medium (Figure 4 and Table 3), which we believe is a consequence of the constitutive expression of OpdA

from pCY76. It has been reported that the apo form of the bacterial phosphotriesterases is considerably less stable [23], and that stabilization of the apo-enzyme enhances the expression of the protein [24]. Because the availability of metal ions in unsupplemented media is considerably less than in supplemented medium, a significantly greater proportion of OpdA expressed under unsupplemented conditions will be in the apo form and therefore less resistant to breakdown, resulting in the production of less soluble protein after 30 h of expression. However, other differences in the growth media cannot be ruled out as the cause of increased expression. It is suspected that the large proportion of apoenzyme present in enzyme purified from unsupplemented medium has contributed to the inability to grow crystals from this preparation, presumably because of the heterogeneity in the protein solution.

The AAS data shows that the relative amount of iron is unchanged and that zinc specifically replaces cobalt in the relative amounts of the three metals when the protein is not expressed in Co^{2+}-supplemented medium. Although this experiment was not able to identify whether the increase in the concentration of zinc had occurred at the α- or β-site, this can be deduced from our prior knowledge from anomalous scattering (Table 2). The anomalous-scattering analysis indicates that the occupancies of the α- and β-sites are dominated by iron and cobalt respectively, and that there is no cobalt present at the α-site. Because the relative concentration of iron and zinc in the medium is unaltered when the enzyme is expressed in, and purified from, unsupplemented medium, the α-site will retain its preference for iron over zinc. Thus, since zinc has replaced cobalt (present only at the β-site), iron should remain the primary constituent of the α-site, with zinc the primary constituent of the β-site. Therefore, although we cannot rule out the possibility that the metal distribution has changed, we think it is highly likely that OpdA expressed in unsupplemented medium contains ∼ 80 % iron at the α-site and ∼ 80 % zinc at the β-site.

The level of phosphotriesterase activity in supplemented medium was approx. 14-fold higher than that in unsupplemented medium, which is in good agreement with the 2.7-fold greater yield of soluble protein and its 5-fold greater specific activity ($2.7 \times 5 = 13.5$) (Table 3). Although the K_m values of OpdA + Co^{2+} (supplemented) and OpdA − Co^{2+} (unsupplemented) are similar, the k_{cat} of OpdA + Co^{2+} is 5-fold higher. While half of the OpdA − Co^{2+} is inactive apoenzyme (see above), this increase in reactivity together with the observation that the α-site is predominantly occupied by iron in both cases (OpdA + Co^{2+} and OpdA − Co^{2+}) does demonstrate that the replacement of zinc by cobalt in the β-site is responsible for the ∼ 2.5-fold improved catalytic efficiency. On the basis of the half-occupancy of OpdA − Co^{2+} (Table 2b), the maximum specific activity of the iron–zinc derivative can be estimated to be ∼ 70 units/mg (Table 3). Approximately one-third of this iron–zinc form also contributes to the activity of OpdA + Co^{2+} (70/3, ∼ 23 units/mg). The remaining activity of OpdA + Co^{2+} ($168 − 23 = 145$ units/mg; Table 3) is expected to be due to the iron–cobalt derivative (Table 2b). Thus, since the Fe-Co derivative comprises approximately two-thirds of OpdA + Co^{2+} (Table 2b) its maximum specific activity is estimated to be ∼ 220 units/mg, approximately three times that of the iron–zinc derivative.

Previous studies on OpdA, and PTE have reported that the metal ions at the α and β positions are responsible for generating the nucleophile and binding the substrates respectively [4,8]. The presence of iron at the α-site thus makes very good sense from a physiological perspective: the pK_A of Fe^{2+}–H_2O is significantly lower than that of Zn^{2+}–H_2O, Co^{2+}–H_2O or Mn^{2+}–H_2O (6.7 versus 9.0, 8.9 and 10.6 respectively [25]),

making it the most efficient Lewis acid in the physiological pH range. Furthermore, enzyme kinetics have demonstrated that the rate-limiting step in the rapid hydrolysis of substrates such as parathion is diffusion, rather than the chemical reaction itself [8,26]. Accordingly, the increased k_{cat} observed here for the Fe-Co derivative of OpdA is consistent with our previous work that demonstrated that the metal ion in the β-site (Co^{2+} or Zn^{2+}) does not significantly affect the reactivity of substrates by differential polarization of the electrophilic phosphorus. Instead, it is proposed that cobalt improves the catalytic efficiency of OpdA toward phosphothionates by increasing the amount of productive substrate binding (affecting the rate of diffusion into the active site) as a consequence of the greater affinity of cobalt for sulphur, compared with zinc [7].

One of the most significant results from the present study is the observation that, in OpdA, phosphotriesterase activity is principally achieved through catalysis by a heterobinuclear iron–cobalt or iron–zinc active site. The combination of X-ray anomalous scattering and AAS measurements demonstrates that cobalt specifically displaces zinc from the β-site of OpdA and does not affect the incorporation of iron into the α-site. These two co-ordination spheres in the active site of OpdA are similar, but not identical. It is impossible to predict the affinity of active sites for different metals, and Co^{2+}, Fe^{2+} and Zn^{2+} are able to be accommodated by a variety of co-ordination geometries [27]. The extra carboxylate ligand in the α-site (Asp^{301}) can affect the metal-ion preference by altering the hard-soft/acid-base characteristics, but, perhaps more significantly, it will also make this co-ordination sphere more symmetrical (Figure 1). It is known that Fe^{2+} has a greater preference for more symmetrical co-ordination than Zn^{2+} or Co^{2+}, which may explain its preference for the α-site. This is also consistent with differences in the co-ordination geometry of the α-site in PTE and OpdA: there is trigonal bipyramidal co-ordination of Zn^{2+} in PTE [5] and octahedral co-ordination of Fe^{2+} in OpdA [4].

Iron is used by a large number of metalloenzymes to catalyse the hydrolysis of phosphate ester bonds. Examples relevant to this study include the purple acid phosphatases from red kidney bean (*Phaseolus vulgaris*) and sweet potato (*Ipomoea batatas*) [28,29], and calcineurin (protein phosphatase 2B) [30]. Red-kidney-bean purple acid phosphatase and calcineurin are believed to contain iron–zinc active sites *in vivo*; however, the oxidation state of their iron ions is different. Purple acid phosphatases contain a tyrosine ligand in the co-ordination sphere of the iron, stabilizing the metal ion in its ferric state. By contrast, calcineurin possesses a histidine residue in an equivalent position, which favours the ferrous state. This has been confirmed through the inactivation of calcineurin through oxidation of Fe^{2+} by superoxide and H_2O_2 [31]. The α co-ordination sphere of OpdA is very similar to that of calcineurin (two water molecules, two carboxylate groups and a histidine residue), which is consistent with our observation that ferrous, not ferric, iron is required for activity (Figure 7).

Our finding that OpdA contains an heterobinuclear iron–zinc active site was somewhat surprising, because PTE (which shares the same six metal co-ordinating amino acid residues, namely His^{55}, His^{57}, Lys^{169}, His^{201}, His^{230} and Asp^{301}) has been described as a naturally occurring zinc enzyme [8]. This assumption was based on 1:1 Zn/enzyme stoichiometry [32], and further analysis indicated that PTE recombinantly expressed in *E. coli* grown in unsupplemented media contained ∼ 1 atom of Zn per protein molecule, and no Co, Mg, Ca or Ni; iron was evidently not tested for [12]. The latter study also reported that the activity of PTE purified in the presence of iron was around 50-fold lower than that for a Zn–Zn enzyme, and 160-fold lower than that for a Co–Co enzyme. This is in contrast with the very high

catalytic efficiency (3.3×10^6 s$^{-1}\cdot$M^{-1}) of the iron-containing OpdA purified in the present study. A possible reason for the low activity of PTE purified in the presence of iron is that the iron may have been predominantly in the ferric state, since no antioxidant was added during purification. This explanation is consistent with the observation that the addition of Fe^{2+} activates OpdA, whereas the addition of Fe^{3+} is inhibitory (Figure 7).

The results we have presented here indicate that the bacterial phosphotriesterase from *A. radiobacter* utilizes a bivalent iron ion at the α-site to generate the nucleophile for the reaction. This result is important, as it indicates that the bacterial phosphotriesterases may be naturally occurring heterobinuclear Fe–Zn enzymes rather than homobinuclear zinc enzymes. Furthermore, it provides evidence that although the structural scaffold of the enzyme is related to the zinc enzyme dihydro-orotase [33] and other members of the amidohydrolase family, the mechanism it utilizes to catalyse phosphate-ester bond hydrolysis has significant similarities to other Fe–Zn binuclear metallophosphatases such as purple acid phosphatase and calcineurin.

REFERENCES

1 Kamanyire, R. and Karalliedde, L. (2004) Organophosphate toxicity and occupational exposure. Occup. Med. (London) **54**, 69–75
2 Horne, I., Sutherland, T. D., Harcourt, R. L., Russell, R. J. and Oakeshott, J. G. (2002) Identification of an *opd* (organophosphate degradation) gene in an *Agrobacterium* isolate. Appl. Environ. Microbiol. **68**, 3371–3376
3 Yang, H., Carr, P. D., McLoughlin, S. Y., Liu, J. W., Horne, I., Qiu, X., Jeffries, C. M., Russell, R. J., Oakeshott, J. G. and Ollis, D. L. (2003) Evolution of an organophosphate-degrading enzyme: a comparison of natural and directed evolution. Protein. Eng. **16**, 135–145
4 Jackson, C., Kim, H. K., Carr, P. D., Liu, J. W. and Ollis, D. L. (2005) The structure of an enzyme–product complex reveals the critical role of a terminal hydroxide nucleophile in the bacterial phosphotriesterase mechanism. Biochim. Biophys. Acta **1752**, 56–64
5 Benning, M. M., Shim, H., Raushel, F. M. and Holden, H. M. (2001) High resolution X-ray structures of different metal-substituted forms of phosphotriesterase from *Pseudomonas diminuta*. Biochemistry **40**, 2712–2722
6 Hong, S. B. and Raushel, F. M. (1996) Metal–substrate interactions facilitate the catalytic activity of the bacterial phosphotriesterase. Biochemistry **35**, 10904–10912
7 Jackson, C. J., Liu, J. W., Coote, M. L. and Ollis, D. L. (2005) The effects of substrate orientation on the mechanism of a phosphotriesterase. Org. Biomol. Chem. **3**, 4343–4350
8 Aubert, S. D., Li, Y. and Raushel, F. M. (2004) Mechanism for the hydrolysis of organophosphates by the bacterial phosphotriesterase. Biochemistry **43**, 5707–5715
9 Sutherland, T. D., Horne, I., Weir, K. M., Coppin, C. W., Williams, M. R., Selleck, M., Russell, R. J. and Oakeshott, J. G. (2004) Enzymatic bioremediation: from enzyme discovery to applications. Clin. Exp. Pharmacol. Physiol. **31**, 817–821
10 Sommerhalter, M., Lieberman, R. L. and Rosenzweig, A. C. (2005) X-ray crystallography and biological metal centers: is seeing believing? Inorg. Chem. **44**, 770–778
11 Ealick, S. E. (2000) Advances in multiple wavelength anomalous diffraction crystallography. Curr. Opin. Chem. Biol. **4**, 495–499
12 Omburo, G. A., Kuo, J. M., Mullins, L. S. and Raushel, F. M. (1992) Characterization of the zinc binding site of bacterial phosphotriesterase. J. Biol. Chem. **267**, 13278–13283
13 Leslie, A. G. W. (1992) Recent changes to the MOSFLM package for processing film and image plate data. Joint CCP4 + ESF-EAMCB Newsletter on Protein Crystallography, no. 26
14 Evans, P. R. (1997) Scaling of MAD data, Proc. CCP4 Study Weekend, 97–102
15 Murshudov, G. N., Vagin, A. A. and Dodson, E. J. (1997) Refinement of macromolecular structures by the maximum-likelihood method. Acta Crystallogr. D **53**, 240–255
16 Collaborative Computational Project, Number 4 (1994) The CCP4 suite: programs for protein crystallography. Acta Crystallogr. D **50**, 760–763
17 Strahs, G. and Kraut, J. (1968) Low-resolution electron-density and anomalous-scattering-density maps of *Chromatium* high-potential iron protein. J. Mol. Biol. **35**, 503–512
18 Emsley, P. and Cowtan, K. (2004) Coot: model-building tools for molecular graphics. Acta Crystallogr. D **60**, 2126–2132
19 Cromer, D. T. and Liberman, D. (1970) Relativistic calculation of anomalous scattering factors for X-rays. J. Chem. Phys. **53**, 1891–1898
19a Brennan, S. and Cowan, P. L. (1992) A suite of programs for calculating X-ray absorption, reflection and diffraction performance for a variety of materials at arbitrary wavelengths. Rev. Sci. Instrum. **63**, 850–853
20 Serdar, C. M., Murdock, D. C. and Rohde, M. F. (1989) Parathion hydrolase gene from *Pseudomonas diminuta* MG: subcloning, complete nucleotide sequence and expression of the mature portion of the enzyme in *Escherichia coli*. Nat. Biotechnol. **7**, 1151–1155
21 Manavathi, B., Pakala, S. B., Gorla, P., Merrick, M. and Siddavattam, D. (2005) Influence of zinc and cobalt on expression and activity of parathion hydrolase from *Flavobacterium* sp. ATCC27551. Pest. Biochem. Physiol. **83**, 37–45
22 Shim, H. and Raushel, F. M. (2000) Self-assembly of the binuclear metal center of phosphotriesterase. Biochemistry **39**, 7357–7364
23 Rochu, D., Viguie, N., Renault, F., Crouzier, D., Froment, M. T. and Masson, P. (2004) Contribution of the active-site metal cation to the catalytic activity and to the conformational stability of phosphotriesterase: temperature- and pH-dependence. Biochem. J. **380**, 627–633
24 Roodveldt, C. and Tawfik, D. S. (2005) Directed evolution of phosphotriesterase from *Pseudomonas diminuta* for heterologous expression in *Escherichia coli* results in stabilization of the metal-free state. Protein Eng. Des. Sel. **18**, 51–58
25 Perrin, D. D. and Dempsey, B. (1974) Buffers for pH and metal ion control, Chapman and Hall, London
26 Caldwell, S. R., Newcomb, J. R., Schlecht, K. A. and Raushel, F. M. (1991) Limits of diffusion in the hydrolysis of substrates by the phosphotriesterase from *Pseudomonas diminuta*. Biochemistry **30**, 7438–7444
27 Greenwood, N. N. and Earnshaw, A. (1997) Chemistry of the Elements, 2nd edn, Butterworth–Heinemann (an imprint of Elsevier Science), Oxford
28 Sträter, N., Klabunde, T., Tucker, P., Witzel, H. and Krebs, B. (1995) Crystal structure of a purple acid phosphatase containing a dinuclear Fe(III)–Zn(II) active site. Science **268**, 1489–1492
29 Schenk, G., Gahan, L. R., Carrington, L. E., Mitić, N., Valizadeh, M., Hamilton, S. E., de Jersey, J. and Guddat, L. W. (2005) Phosphate forms an unusual tripodal complex with the Fe–Mn center of sweet potato purple acid phosphatase. Proc. Natl. Acad. Sci. U.S.A. **102**, 273–278
30 Kissinger, C. R., Parge, H. E., Knighton, D. R., Lewis, C. T., Pelletier, L. A., Tempczyk, A., Kalish, V. J., Tucker, K. D., Showalter, R. E., Moomaw, E. W. et al. (1995) Crystal structures of human calcineurin and the human FKBP12–FK506–calcineurin complex. Nature (London) **378**, 641–644
31 Namgaladze, D., Hofer, H. W. and Ullrich, V. (2002) Redox control of calcineurin by targeting the binuclear Fe^{2+}–Zn^{2+} center at the enzyme active site. J. Biol. Chem. **277**, 5962–5969
32 Dumas, D. P., Caldwell, S. R., Wild, J. R. and Raushel, F. M. (1989) Purification and properties of the phosphotriesterase from *Pseudomonas diminuta*. J. Biol. Chem. **264**, 19659–19665
33 Thoden, J. B., Phillips, Jr, G. N., Neal, T. M., Raushel, F. M. and Holden, H. M. (2001) Molecular structure of dihydroorotase: a paradigm for catalysis through the use of a binuclear metal center. Biochemistry **40**, 6989–6997